ELSEVIER

Journal of Electron Spectroscopy and Related Phenomena 123 (2002) 333–344

JOURNAL OF ELECTRON SPECTROSCOPY and Related Phenomena

www.elsevier.com/locate/elspec

Particle-in-a-box momentum densities compared with electron momentum spectroscopy measurements

Maarten Vos*, Erich Weigold

Atomic and Molecular Physics Laboratories, Research School of Physical Sciences and Engineering, The Australian National University, Canberra ACT 0200, Australia

Received 21 August 2001; received in revised form 16 December 2001; accepted 3 January 2002

Abstract

We investigate the momentum space representation of the solutions of a particle in a three-dimensional box. By comparing the calculated momentum densities of a particle in a box with the measured distribution of highly symmetric molecules we want to elucidate the nature of the measured orbitals. Finally the measured momentum distribution of a free electron metal is compared with the results of this model. © 2002 Elsevier Science B.V. All rights reserved.

Keywords: Momentum densities; Methane; Cubane; Aluminum

1. Introduction

Electron momentum spectroscopy (EMS) is a tool that is able to measure state-selected momentum densities in atoms, molecules and solids [1–3]. These measured momentum densities are proportional to the modulus square of the wave function in momentum space, and therefore EMS results are among the most direct experimental information about the electron wave function one can obtain. There is thus a firm basis of comparing EMS results with theoretical calculations. An intuitive understanding of these data is hampered, however, by the fact that one visualises the wave function in coordinate space, rather than momentum space. In order to overcome this problem it is helpful to consider very simple models. In the past we discussed extensively the momentum densities of fictitious, linear hydrogen chains [4], as well as the effect of chemical bonding on the observed momentum densities [5]. Here we want to extend this series to a simple three-dimensional model, of electrons in a cubic box. In the case of a small number of electrons in a small box we compare it with the measured momentum densities of highly symmetric molecules [6,7]. In the limit of a large box, with many electrons, the model calculations are compared to a free electron metal [8,9].

The model used here is of course not new. In solid state physics the free electron model is the standard starting point for the understanding of simple metals (e.g., Refs. [10,11]). In quantum chemistry a similar approach is used in the free electron molecular orbital (FEMO) model (e.g., Ref. [12]), but here it is usually restricted to the description of the energy

*Corresponding author. Tel.: +61-2-6125-4985; fax: +61-2-6125-2452.
E-mail address: maarten.vos@rsphysse.anu.edu.au (M. Vos).

0368-2048/02/$ – see front matter
PII: S0368-2048(02)00031-2

levels of the π electrons in organic molecules. In this paper we use it to describe all valence electrons. We focus on the momentum space solution of the particle-in-a-box problem, and see to what extent this approach is useful in understanding orbital momentum densities which are measured by electron momentum spectroscopy.

2. The Model

2.1. One-dimensional box

In Fig. 1 we plot the solution of the Schrödinger equation in a one-dimensional box, extending from $-a$ to a. The potential inside the box is 0, outside the box ∞. The coordinate space solutions are the familiar (e.g., Ref. [13]):

$$\psi_n(x) = \frac{1}{\sqrt{a}} \cos\left(\frac{n\pi x}{2a}\right) \tag{1}$$

for $n = 1,3,5\ldots$ and

$$\psi_n(x) = \frac{1}{\sqrt{a}} \sin\left(\frac{n\pi x}{2a}\right) \tag{2}$$

for $n = 2,4,6\ldots.$ and the (kinetic) energy of these states is

$$E = \frac{\pi^2\hbar^2 n^2}{8ma^2} \tag{3}$$

The momentum space wave functions $\phi(p_x)$ are obtained by Fourier transform:

$$\phi_n(k) = \frac{1}{\sqrt{2\pi\hbar}} \int_{-a}^{a} \psi_n(x) e^{ikx}\, \mathrm{d}x$$

$$= \frac{1}{\sqrt{2\pi\hbar}} \int_{-a}^{a} \psi_n(x)(\cos(kx) + i\sin(kx))\mathrm{d}x.$$

For the even $\psi_n(x)$ (i.e., $n =$ odd!) the Fourier transform is real. If $\psi_n(x)$ is odd the sin() term will

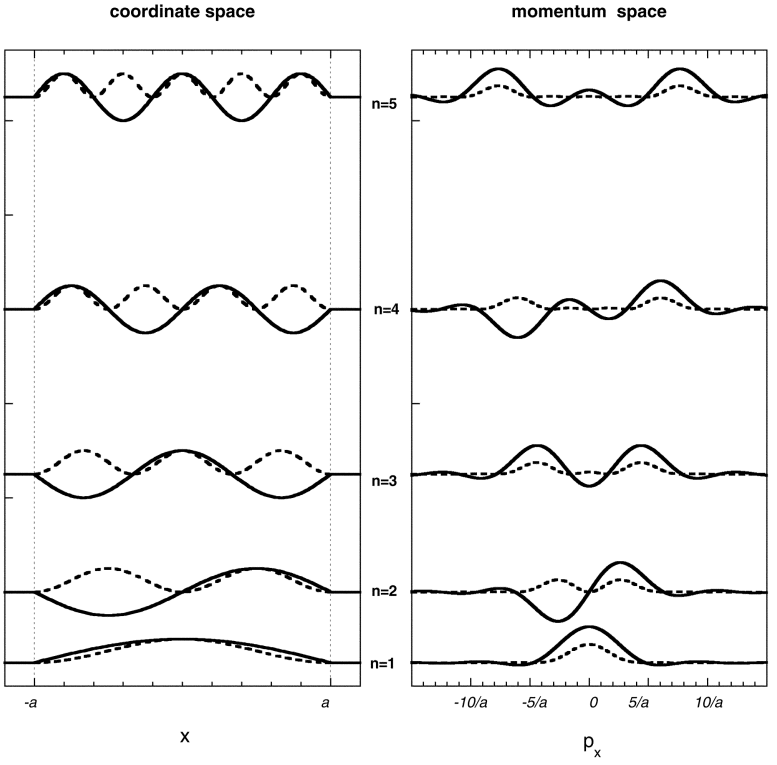

Fig. 1. The first five solutions of a particle in a box, both in coordinate space (left) and momentum space (right). The wave function ($\psi(x)$ coordinate space, $\phi(p_x)$ momentum space, are plotted as a solid line, the densities (modulus square of the wave function) as a dashed line.

contribute and the Fourier transform is along the imaginary axis. These transforms are completely straight forward. For example for n is odd we get ($|k| \neq \frac{n\pi}{2a}$):

$$\phi_n(k) = \frac{1}{\sqrt{2\pi\hbar a}} \int_{-a}^{a} \cos\left(\frac{n\pi x}{2a}\right) \cos(kx)\mathrm{d}x$$
$$= \frac{\sqrt{2a}}{\sqrt{\pi}\hbar} \left[\frac{1}{n\pi + 2ak} + \frac{1}{n\pi - 2ak} \right] \times \sin\left(\frac{n\pi}{2}\right) \cos(ka),$$

and

$$\phi_n\left(\pm\frac{n\pi}{2a}\right) = \frac{2a}{\sqrt{2\pi\hbar a}}.$$

Similar results for obtained for n even.

The results are plotted in Fig. 1. For convenience we omitted the phase factor i. In this figure the solutions are offset vertically by an amount proportional to their kinetic energy. For all n the intensity of $\psi(x) = 0$ for $|x| \geq a$. However, for $\phi(p_x)$ there are no such limitations. The value of p_x corresponding to the maximum momentum density will increase approximately linearly with n.

Most plots in this paper use atomic units (a.u.). In this system $\hbar = 1$, the mass of the electron $m = 1$ and the elemental charge $e = 1$. A length of 1 a.u. corresponds to the Bohr radius, 0.529 Å. One a.u. of momentum is 1.89 $Å^{-1}$. The unit of energy in this system is the Hartree. 1 Hartree $\simeq$27.21 eV.

2.2. Two-dimensional box

The different degrees of freedom for a square box ($V = 0$ if $-a < x < a$ and $-a < y < a$, $V = \infty$ elsewhere) do not couple in the Schrödinger equation. Hence the solution in two dimensions is just the product of the solutions in one dimension. Again the momentum representation is obtained by Fourier transform:

$$\frac{1}{2\pi\hbar} \int_{-a}^{a} \int_{-a}^{a} \psi_{n_x}(x)\psi_{n_y}(y) e^{ik_x x} e^{ik_y y}\, \mathrm{d}x\, \mathrm{d}y$$
$$= \frac{1}{\sqrt{2\pi\hbar}} \int_{-a}^{a} \psi_{n_x}(x) e^{ik_x x}\, \mathrm{d}x \frac{1}{\sqrt{2\pi\hbar}} \int_{-a}^{a} \psi_{n_y}(y) e^{ik_y y}\, \mathrm{d}y$$
$$= \phi_{n_x}(k_x)\phi_{n_y}(k_y).$$

Thus, in momentum representation the two-dimensional solution is also a product of the one-dimensional solutions. Each solution has an energy given by

$$E = \frac{\pi^2\hbar^2(n_x^2 + n_y^2)}{8ma^2}.$$

In Fig. 2 we plot the solutions of the densities (i.e., the modulus square of the wave function) in two dimensions as a grey scale plot for the first six solutions. The coordinate space plot dimension corresponds to the box size, it extends from $-a$ to a in both dimensions. The momentum space plot is from $-8/a$ to $8/a$. The latter choice is somewhat arbitrarily, as the momentum density only approaches zero for large momentum values. In the figure the notation (n_x,n_y) refers to the solution $\psi_{n_x}(x)\psi_{n_y}(y)$ in coordinate space or $\phi_{n_x}(k_x)\phi_{n_y}(k_y)$ in momentum space.

As an example for solution (1,2) the $x-$function is even, and the $y-$function is odd. This means that for the line for which $y = 0$ the wave function changes sign and thus the density is zero. Similarly the momentum representation of (1,2) displays zero intensity for $p_y = 0$. It is obvious from Fig. 2 that the same symmetries apply to the momentum representation as to the coordinate representation. However the shape of the distributions in coordinate space and momentum space are completely different. For the higher order solution the intensity of the momentum density near $(p_x = 0, p_y = 0)$ is always extremely small, and the position of the maxima of the momentum density distribution increases with increasing n_x,n_y, whereas the coordinate space representation remains more evenly spread out over the whole box.

Interestingly the (3,1) and (1,3) solutions discussed above can be transformed into a more symmetric representation. This is explained in Fig. 3. In these cases the solution of the wave function is symmetric along $x = 0$ ($p_x = 0$) and $y = 0$ ($p_y = 0$). By taking a linear combination:

$$\psi_s^{(3,1)} = \frac{1}{\sqrt{2}}((3,1) + (1,3)) \quad (4)$$

and

$$\psi_a^{(3,1)} = \frac{1}{\sqrt{2}}((3,1) - (1,3)) \quad (5)$$

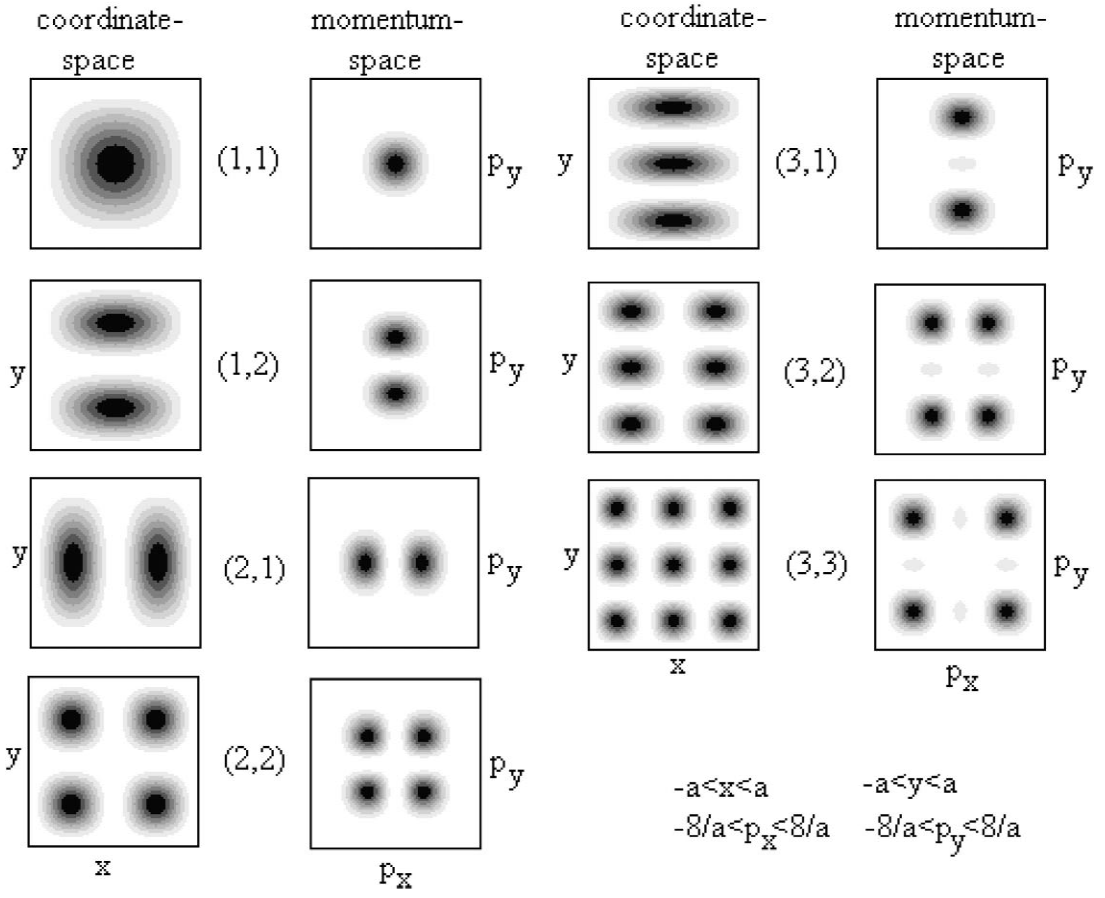

Fig. 2. The first solutions of a particle in a square, two-dimensional box. The modulus square of the wave functions ($|\psi(x,y)|^2$ in coordinate space, $|\phi(p_x,p_y)|^2$ in momentum space) are plotted as grey-scale plots, the darker shades corresponding to larger densities.

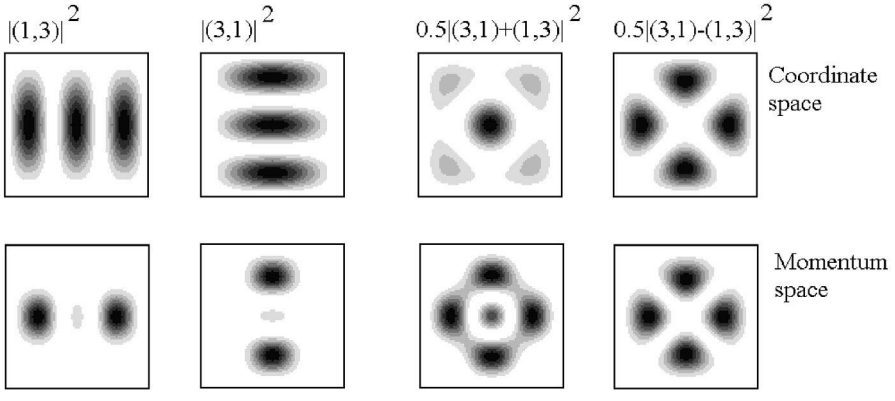

Fig. 3. Construction of the most symmetric solutions out of the (3,1) and (1,3) solutions.

we obtain solutions that, in addition to the symmetry operations mentioned above, are symmetric ($\psi_s^{(3,1)}$) and antisymmetric ($\psi_a^{(3,1)}$) along the line $x = y$ and $x = -y$. The same transformation can be done in momentum space.

For electrons in a box both solutions have the same energy. If, however, we would have a varying potential this degeneracy could be lifted. For example changing the potential (while maintaining the 4-fold symmetry axis) along the lines ($x = y, x = -y$) would affect the energy of the symmetric solution $\psi_s^{(3,1)}$ much more than the anti-symmetric one $\psi_a^{(3,1)}$.

The above procedure would not work for the (2,1) solution, as it involves functions which are symmetric in one dimension and anti-symmetric in the other dimension. Thus taking combinations as in Eqs. (4) and (5) would destroy the symmetry along $x = 0$ and $y = 0$.

2.3. Three-dimensional box

The extension to a three-dimensional box is straight forward. The solutions are now the product of three components. We now want to compare the distributions with those measured for symmetric molecules. Unfortunately these molecules have random orientation in the gas phase. Most EMS spectrometers are arranged in such a way, that by measuring coincident count rates at different detector angles the momentum density along a line (p'_x,0,0), with p'_x a fixed direction relative to the spectrometer, is obtained. Thus, these lines are along different directions of the coordinate system of the randomly oriented molecules. This means that we have to average the calculated momentum density over all directions, in order to compare with the experiment.

$$I_{\text{obs.}}(p') = \int_0^{2\pi}\int_0^{\pi} |\phi_{xyz}(p'\sin(\theta)\cos(\phi),\, p'\sin(\theta)\sin(\phi),\, p'\cos(\theta))|^2 \sin(\theta)\,\mathrm{d}\theta\,\mathrm{d}\phi \quad (6)$$

The results are shown in Fig. 4 for a box containing 40 electrons, and a size of 10 a.u. These momentum densities are offset by an amount proportional to the kinetic energy of each state. These

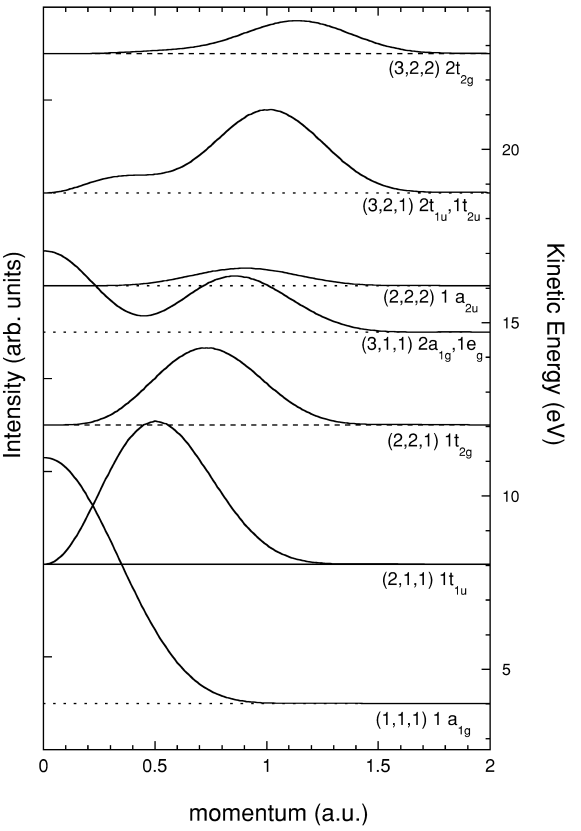

Fig. 4. The first seven (spherically averaged) momentum densities of a cubic box of dimension 10 a.u. Each momentum density is multiplied by its degeneracy and offset by an amount proportional to its kinetic energy.

densities are multiplied by the degeneracy of each orbital (degeneracy 1 for (1,1,1) and (2,2,2), 3 for (2,1,1), (2,2,1), (3,1,1) and (3,2,2), 6 for (3,2,1)). Thus there are 20 states each occupied by two electrons (spin up, spin down). In general we have again that the momentum density peaks at larger and larger values with increasing energy. A notable exception is the (3,1,1) state. It peaks again at zero momentum. In the two-dimensional case we saw that the maximum density of the (3,1) function is not at ($p_x = 0,\ p_y = 0$). Neither is the maximum at zero momentum for the three-dimensional case. However for each (θ,ϕ) value in Eq. (6) the density at zero momentum contributes to $I_{\text{obs.}}(0)$, whereas only for specific (θ,ϕ) directions will the part of the wave function with maximum density contribute to

$I_{\text{obs.}}(p')$. Thus the maximum at zero momentum for the (3,1,1) case is a consequence of the required spherical averaging.

Again we can transform some solutions (orbitals) into a representation that emphasises the symmetry. In the (3,1,1) case we can construct one ($1a_{1g}$) orbital with the full cubic symmetry:

$$\frac{1}{\sqrt{3}}(\psi_{311} + \psi_{131} + \psi_{113}) \tag{7}$$

and two equivalent ($1e_g$) orbitals:

$$\frac{1}{\sqrt{2}}(\psi_{311} - \psi_{131}) \tag{8}$$

$$\frac{1}{\sqrt{6}}(2\psi_{113} - \psi_{311} - \psi_{131}) \tag{9}$$

As is evident from Fig. 5 these orbitals have rather different momentum distributions. The orbital with the full cubic symmetry is the only one with intensity at zero momentum. If the square box is replaced by a nonuniform potential with cubic symmetry we would expect the (311) levels to split, with only a single, non-degenerate orbital having intensity at zero momentum.

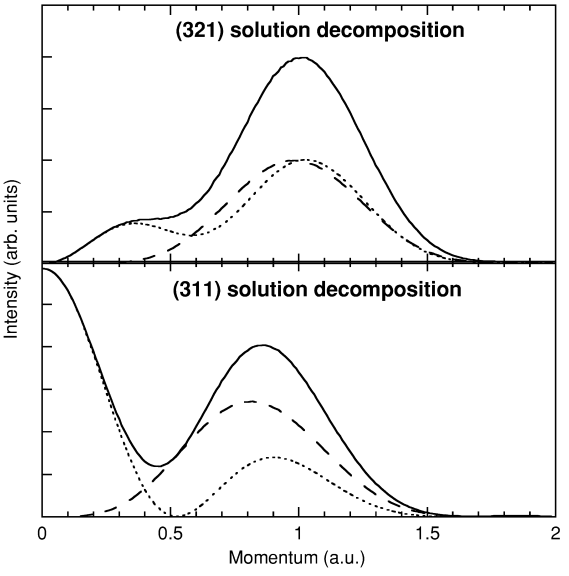

Fig. 5. Decomposition of the (3,1,1) and (3,2,1) solutions into solutions of maximum symmetry. The three (3,1,1) solutions can be decomposed into one with the full cubic ($2a_{1g}$) symmetry (dotted line), and two with lower symmetry ($1e_g$) (dashed line) Similarly the six (321) solutions can be decomposed into three $2t_{1u}$ (dotted line) and three $2t_{2u}$ solutions (dashed line).

The 6-fold degenerate (3,2,1) orbital can be decomposed as well. Consider the following pairs:

$$\frac{1}{\sqrt{2}}(\psi_{321} + \psi_{123}), \quad \frac{1}{\sqrt{2}}(\psi_{321} - \psi_{123}) \tag{10}$$

The left function is symmetric for reflections along the plane $x = z$ (t_{1u} type orbital), the right one anti-symmetric (t_{2u} type orbital). Similarly we can construct:

$$\frac{1}{\sqrt{2}}(\psi_{231} + \psi_{213}), \quad \frac{1}{\sqrt{2}}(\psi_{231} - \psi_{213})$$

$$\frac{1}{\sqrt{2}}(\psi_{132} + \psi_{312}), \quad \frac{1}{\sqrt{2}}(\psi_{132} - \psi_{312})$$

with similar symmetries for the $x = y$ and $y = z$ plane. Spherically averaged all three symmetric distributions are equivalent, but they differ from the three anti-symmetric ones, as shown in Fig. 5.

3. Comparison with experiment

3.1. Methane

Methane has been a popular target as it is a highly symmetric simple organic molecule. It does not have the full cubic symmetry (only every second corner of a cube is occupied by hydrogen), but this will not cause a splitting of the innermost levels. Methane has been measured by Hood et al. [14], Weigold et al. [15] and by Clark et al. [7]. Here we compare the the measured momentum distributions by Clark et al. with the simple model presented here (see Fig. 6). The size of the box was used as a fitting parameter and chosen to be 8 a.u. (i.e., $a = 4$ a.u.). The same scaling factor was used to compare theory and experiment for the inner and outer orbital. No attempt was made to fold the theory with the experimental momentum resolution. In spite of this, our rough theory predicts the shapes and intensities reasonably well. The excess intensity of the experiment for the outer orbital at zero momentum is due to finite momentum resolution. It is the excess intensity at high momentum that is due to the potential of the nuclei. Near the nuclei the wave

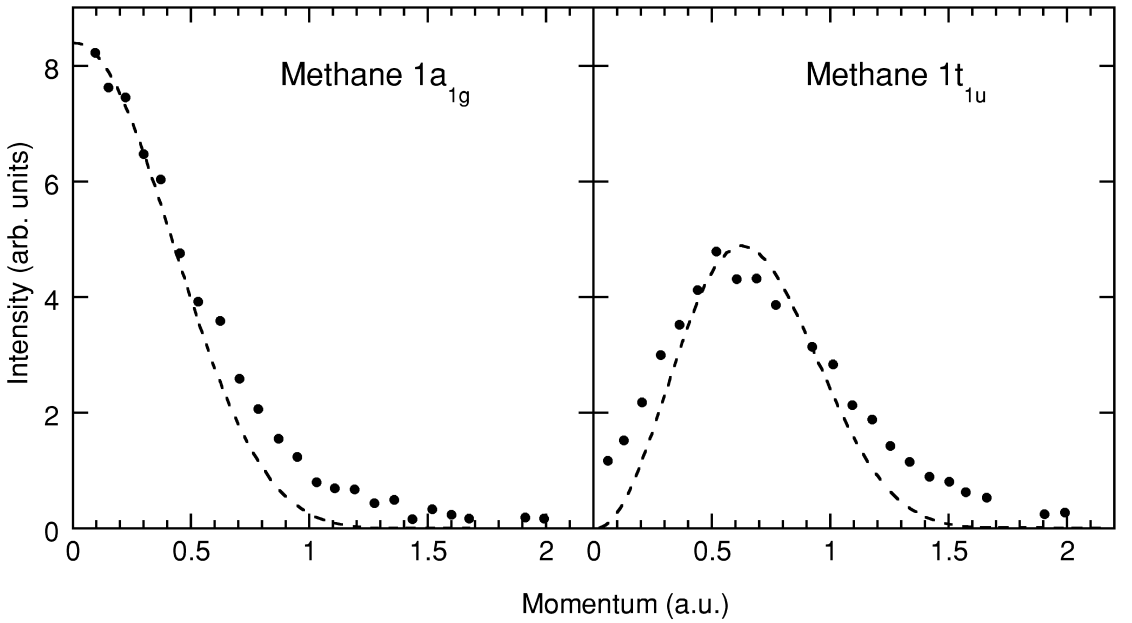

Fig. 6. The measured momentum distribution for the inner ($1a_{1g}$) and outer ($1t_{1u}$) valence orbitals of methane as measured by Clark et al. [7] compared to that derived for the two lowest energy solutions of a particle in a box of size 8 a.u. The intensity of the $1t_{1u}$ orbital was multiplied by three in order to take into account the degeneracy. For both orbitals the same scaling factor is used for comparison of the theory and experiment.

function will vary quickly, and this will cause a high momentum contribution to the density. This is obviously not included in the model. The energy difference between both levels is predicted to be 6.3 eV by our simple model, whereas the experimentally obtained value is 8.92 eV [7].

3.2. Cubane

The agreement of the model for methane could be somewhat fortuitous, as we fit two curves with two fitting parameters (box size and a single intensity scaling factor). An ideal test case is cubane (C_8H_8) as it has has the full cubic symmetry (see Fig. 7). It was measured by Adcock et al. [6]. In a cubic box the 40 valence electrons will occupy nine different levels, the molecular symmetries of which are indicated in Fig. 4.

Both in our model and in the experiment there are two orbitals with density at zero momentum. Also both in the model and experiment there is a general trend of the orbitals peaking at higher momentum with decreasing binding energy. The experimental data and model calculations are plotted together in Fig. 8. For all orbitals the same scaling factor was used for comparing the measured and calculated

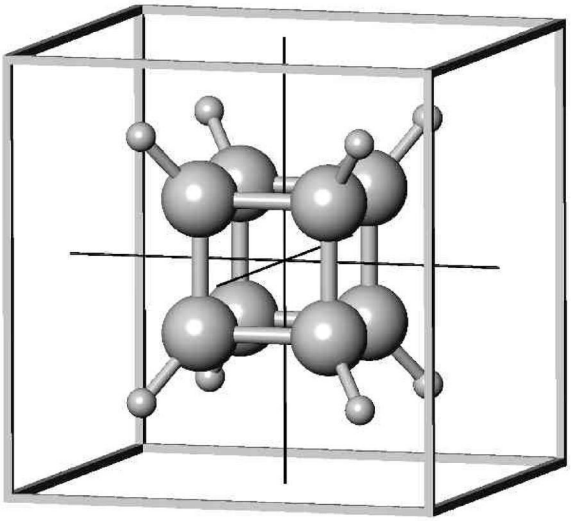

Fig. 7. The molecule cubane (C_8H_8) together with the box used to model it.

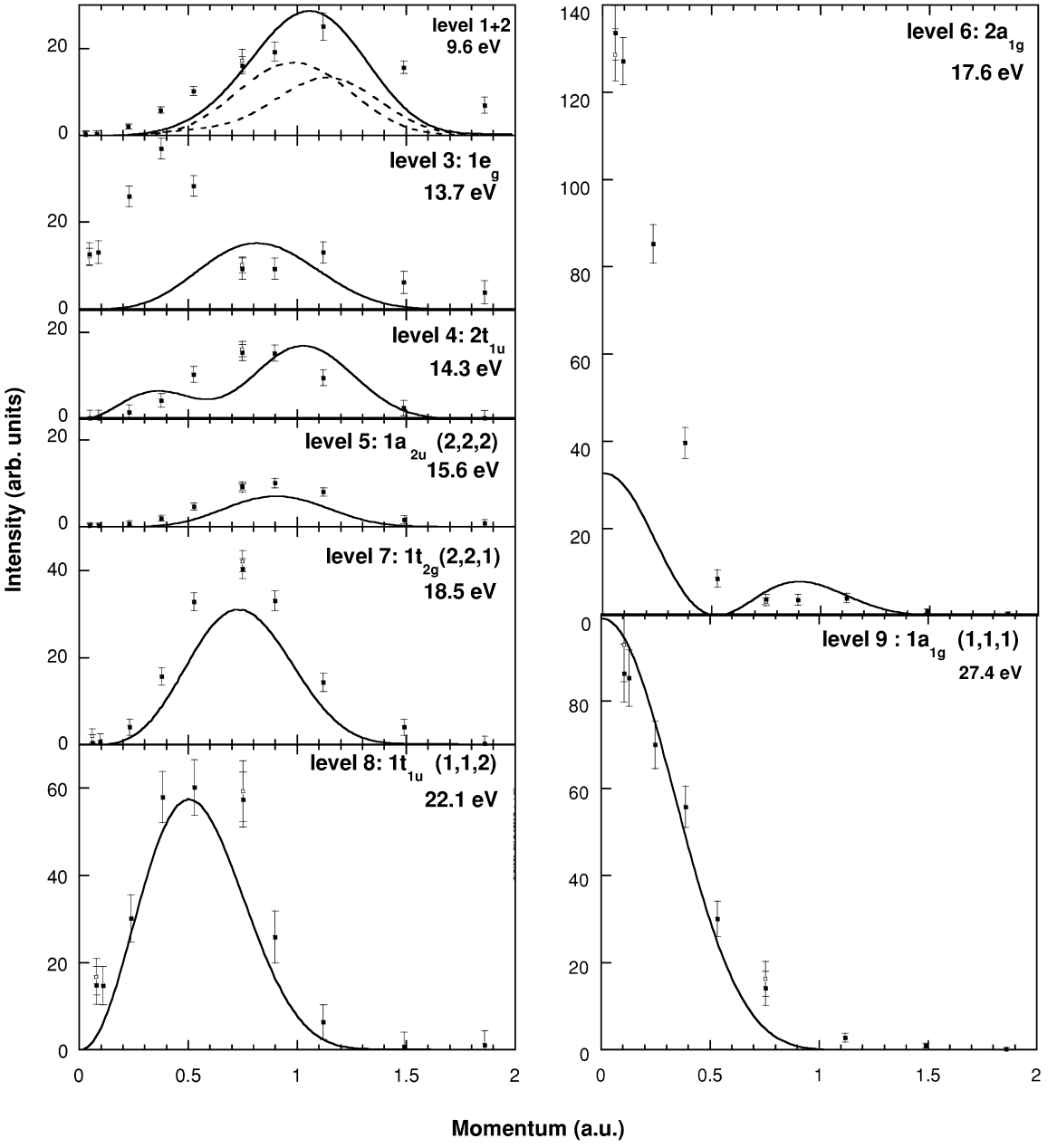

Fig. 8. The measured spectra of cubane compared to the momentum profiles derived from a model calculations of a particle in a cubic box of size 10 a.u. Level one and two were not resolved in the experiment. The observed binding energies are indicated as well.

intensity. The size of the box is 10 a.u. (i.e., $a = 5$ a.u.), the same as in Section 2.3. This is the other 'fitting' parameter. Most orbitals are described semi-quantitatively by this simple model. The noticeable exception are the $1e_g$ and $2a_{1g}$ orbitals, both derived from the (311) solution. The momentum profile of these orbitals seems to be most influenced by the changes of the potential in the box due to the positioning of the nuclei. This is also clear from the large separation in energy (4.1 eV) found experimen-

tally [6], whereas these orbitals are degenerate within our simple model.

The binding energies of cubane span a range of 17.8 eV [6], whereas our simple model predicts a (kinetic) energy range of 18.8 eV energy. The potential energy in our model is zero everywhere inside the box. Thus the model suggests that most orbitals are affected in a similar way by the potential energy, and that kinetic energy is the main cause of the difference in energy between orbitals.

Modern quantum-chemistry calculations describe the experimental data very well [6]. The model calculations described here may be a good starting point for obtaining an intuitive understanding of the observed distributions and the role of the global symmetry (cubic) in determining orbital shapes.

4. Aluminum

If we increase the size of the box the width of the momentum density of each orbital will decrease proportionally (see Fig. 1), and the energy separation between different levels becomes smaller (Eq. (3)). If we keep the electron density constant, then larger boxes will have more occupied orbitals. The momentum density of almost all these orbitals will peak at a momentum value close to $\sqrt{2E}$ with E the kinetic energy in Hartrees. If the level separation is smaller than the energy resolution one measures a continuous distribution. Its shape depends only on the density of electrons, not on the size of the sample. In this limit the free electron model for molecules evolves into the familiar free electron model of a solid [11].

An example for an aluminum film is given in Fig. 9. There are very sharp peaks in the momentum distribution, especially near the Fermi level. These peaks are at decreasing momentum values with increasing binding energy, and reach $k = 0$ at a binding energy of 12 eV. Here the kinetic energy is zero, and the 12 eV binding energy is due to the interaction with the positive ion cores. The kinetic energy of the electrons is thus close to $12 - E_{\mathrm{bind}}$, and the momentum distribution should thus peak at $\sqrt{2(12 - E_{\mathrm{bind}})/27.21}$ (E_{bind} in eV). These momentum values are indicated by arrows in Fig. 9. The free electron model predicts the peak position very well. Similar conclusions are reached using angular-resolved photoemission [16].

From the density of electrons in aluminum we expect a Fermi vector k_f of 0.93 a.u. [11]. The measured value of $\simeq 0.88$ a.u. is slightly less, but entirely consistent with the value of 0.93, if one takes into account the effect of finite energy resolution ($\simeq 1.8$ eV) which causes a range of orbitals near the Fermi level to be sampled, all peaking at energies $\leq k_f$. The aluminum valence band is thought to be formed by two 3s and one 3p electron per nucleus. The dominant features of the valence band spectra can be understood by considering only the density of particles in the box, and the nature of the 3s and 3p parent orbitals is not reflected directly in the measured densities.

In Fig. 10 we show the energy-integrated momentum density of cubane and aluminum. For a free-electron solid (in the independent electron approximation and at $T = 0$) the momentum density is constant up until the Fermi vector k_f is reached and vanishes for larger momenta. k_f is given by

$$k_f = \frac{1.92}{r_s}$$

with r_s the radius of a sphere with the same volume as the volume per electron in the solid [11]. For aluminum the experiment displays a rather constant momentum density below k_f followed by a steep decline and a tail extending to higher momentum values. This high-momentum tail is partly due to electron–electron correlation and partly due to elastic multiple scattering as discussed in Ref. [9]. For cubane the limit of an infinitely large solid has not been reached. Both the model calculation and the experiment do not show a constant momentum density for small values of k. However, the value of steepest decline coincides approximately (both in the model calculation and the experiment) with the value of k_f derived from the electron density of the model.

5. Discussion and conclusion

We have explored the extremely simple ‘free electron model’ of molecules and solids. Considering its crudeness it is extremely successful in describing the observed momentum profiles for systems with

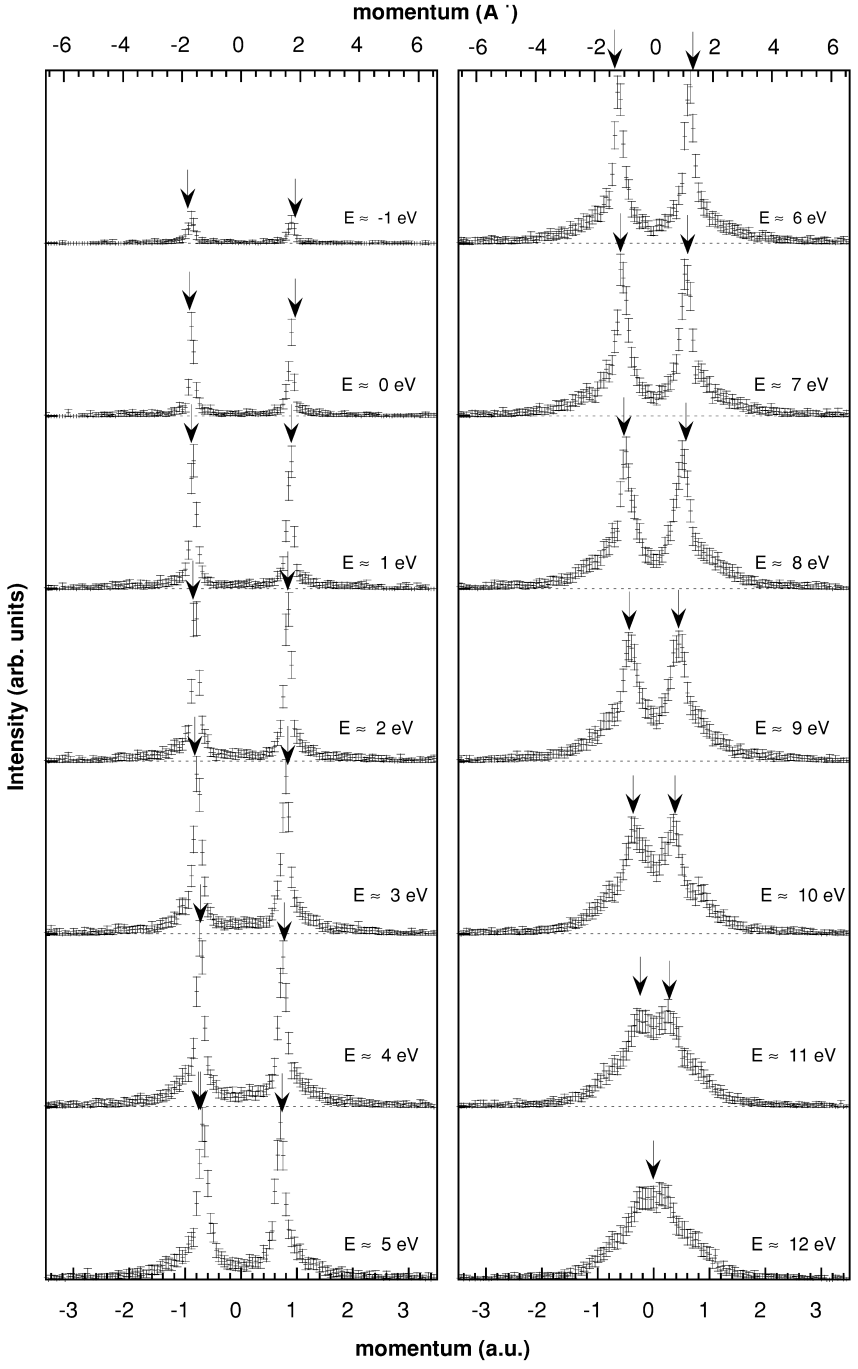

Fig. 9. Momentum densities of aluminum at selected binding energies. The momentum positions corresponding to $k=\sqrt{2mE_{\mathrm{kin}}}$ (E_{kin} in Hartrees) are indicated by arrows, assuming $E_{\mathrm{kin}}=0$ at the binding energy of 12 eV.

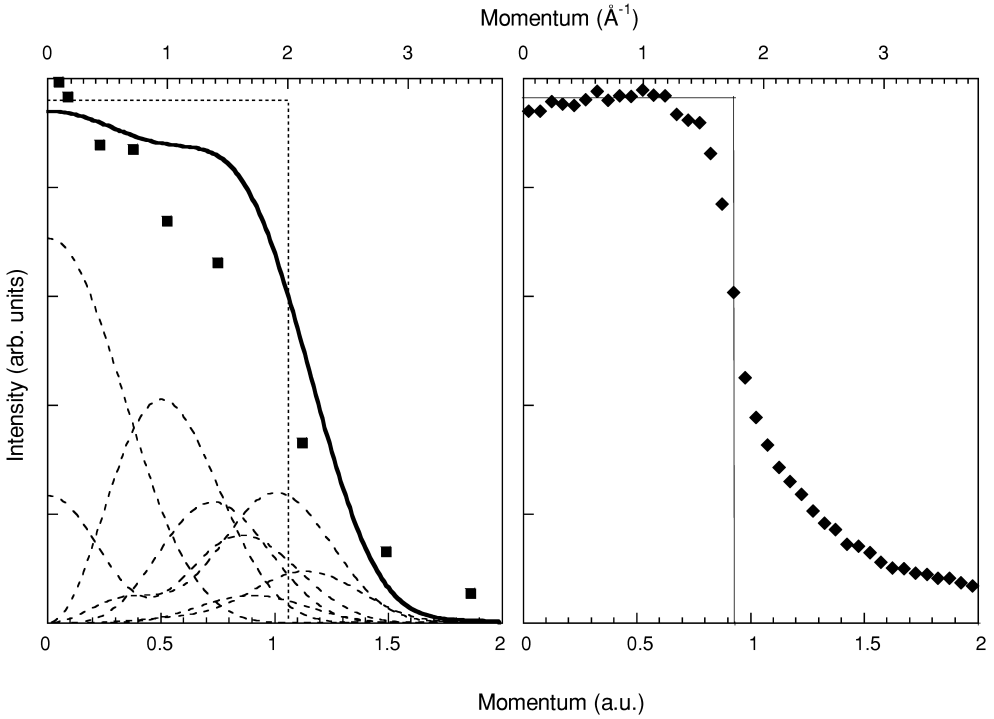

Fig. 10. Energy-integrated momentum density of cubane (left) and aluminum (right). For cubane we show the calculated individual orbitals as dotted lines, the sum of the calculated orbitals as the full line. Squares are the integrated experimental results. The dotted line is the momentum density of a free electron solid with the same electron density as the cubane model calculation (40 electrons/1000 (a.u.)^3). The right panel shows the aluminum data and the momentum density of a free-electron solid with the same electron density as the aluminum valence band.

cubic symmetry, and it even describes roughly the energy separation of the different orbitals, especially for the larger systems. One of the surprising elements is that these results are obtained even though the model completely neglects the nature of the atomic 'parent' orbitals, for example their s and p character. EMS spectra display their most salient features at low momentum ($|p| \leq 1$ a.u.). This corresponds to phase changes in the wave function in coordinate space over distances larger than 1 a.u., i.e., of the order of or slightly less than the atomic separation. It appears that, at least for the low momentum range, the nature of the parent orbital is of secondary importance, compared with the influence of the molecular size, geometry and hence symmetry. Near a nucleus the Z/r Coulomb potential of a single atom will dominate, and there the symmetry of the potential will approach the spherical symmetry of an atom. It is there, and only there, that the solutions approach s- and p-type orbitals. These short range fluctuation of $\psi(x)$ near a nucleus will result in high-momentum components of the $\phi(p)$ solution. The corresponding intensity at any given point is low, and hence does not noticeably affect the overall shape of the measured momentum distributions.

The structure of the calculated orbital in the 'free electron molecule model' described has its roots in the requirement that each orbital should be orthogonal to the other orbitals. This causes nodes in the wave function that for symmetric molecules, more often than not, pass through the origin, both in coordinate and momentum space and then the resulting orbitals appear 'p' like. In this light it is interesting to see what happens if we distort the symmetry of a cluster. For example Bawagan and Brion measured the outer valence band of NH_3 and CH_3NH_2 [17]. For the highly symmetric NH_3 mole-

cule the outer valence orbital has a node at the origin, and hence low intensity at zero momentum was found. A reduction of the symmetry by replacing one H atom by a CH_3 group caused a noticeable increase of the intensity at zero momentum. Within a 'chemical' interpretation of the EMS data this is referred to as increased s character of the outer valence orbital. Within the 'free-electron model' described here one would expect the same trend, but explain it as movements of the orbital nodes due to the reduced symmetry, both in real and momentum space. For many orbitals this will lead to an increase in the observed intensity at zero momentum.

In conclusion, extremely simple model calculations allow us to describe a range of systems on a semi-quantitative level. We consider it useful as a starting point for obtaining an intuitive understanding of the observed distributions. Fully quantitative descriptions of the results can only be obtained by high-quality quantum mechanical calculations. The model highlights the extended nature of the orbitals, and stresses the importance of the symmetry of the system. It seems to indicate that momentum densities of the valence electrons are not directly related to the wave functions of free atoms that are the building blocks of the compounds.

Acknowledgements

The authors want to thank Dr. M. Brunger for making the cubane data available, Mr G. Cornish for assisting with the drawings, and Dr. V. Sashin for critically reading the manuscript.

References

[1] I. McCarthy, E. Weigold, Electron momentum spectroscopy of atoms and molecules, Rep. Prog. Phys. 54 (1991) 789.
[2] E. Weigold, I. McCarthy, in: Electron Momentum Spectroscopy, Kluwer Academic/Plenum, New York, 1999.
[3] C. Brion, G. Cooper, Y. Zheng, I. Litvinyuk, I. McCarthy, Imaging of orbital electron densities by electron momentum spectroscopy, a chemical interpretation of the binary (e,2e) reaction, Chem. Phys. 270 (13) (2001) 13–30.
[4] M. Vos, I. McCarthy, Observing electron motion in solids, Rev. Mod. Phys. 67 (1995) 713.
[5] M. Vos, I. McCarthy, Measuring orbitals and bonding in atoms, molecules and solids, Am. J. Phys. 65 (6) (1997) 544.
[6] W. Adcock, M. Brunger, I. McCarthy, M. Michalewicz, W. von Niessen, F. Wang, E. Weigold, D. Winkler, A density functional and electron momentum spectroscopy study into the complete valence electron structure of cubane, J. Am. Chem. Soc. 122 (2000) 3892–3900.
[7] S. Clark, T. Reddish, C. Brion, E. Davidson, R. Frey, Momentum distributions and binding energy spectra of CH_4, Chem. Phys. 143 (1990) 1.
[8] M. Vos, A. Kheifets, E. Weigold, Momentum profiles of aluminum, J. Electron Spectrosc. Relat. Phenom. 114–116 (2001) 1031–1036.
[9] M. Vos, A. Kheifets, E. Weigold, The spectral momentum density of aluminum measured by electron momentum spectroscopy, J. Phys. Chem. Solids 62 (2001) 2215.
[10] C. Kittel, in: Introduction to Solid State Physics, 6th Edition, Wiley, New York, 1986.
[11] N. Ashcroft, N. Mermin, in: Solid State Physics, Holt-Saunders, New York, 1976.
[12] F. Pilar, in: Elementary Quantum Chemistry, McGraw-Hill, New York, 1968.
[13] S. Gasiorowicz, in: Quantum Physics, Wiley, New York, 1974.
[14] S. Hood, E. Weigold, I. McCarthy, P. Teubner, Momentum space wave functions and binding energies of the valence electrons in methane measured by the (e,2e) technique, Nat. Phys. Sci. 245 (144) (1973) 65–68.
[15] E. Weigold, S. Dey, A. Dixon, I. McCarthy, P. Teubner, (e,2e) spectroscopy of methane, Chem. Phys. Let. 41 (1) (1976) 21–24.
[16] L. Levinson, F. Greuter, E. Plummer, Phys. Rev. B 27 (1983) 727.
[17] A. Bawagan, C. Brion, Studies of the electron density in the outermost orbitals of NH_2CH_3, $NH(CH_3)_2$, $N(CH_3)_3$ and NF_3 by electron momentum spectroscopy: evidence for charge delocalization, Chem. Phys. 123 (1988) 51.